SAND2022-10852J

ECS Journal of Solid State
Science and Technology

The Electrochemical Society
Advancing solid state & electrochemical science & technology

Surface Functionalized Barium Titanate Nanoparticles: A Combined Experimental and Computational Study

To cite this article: Jessica N. Domrzalski *et al* 2022 *ECS J. Solid State Sci. Technol.* **11** 063006

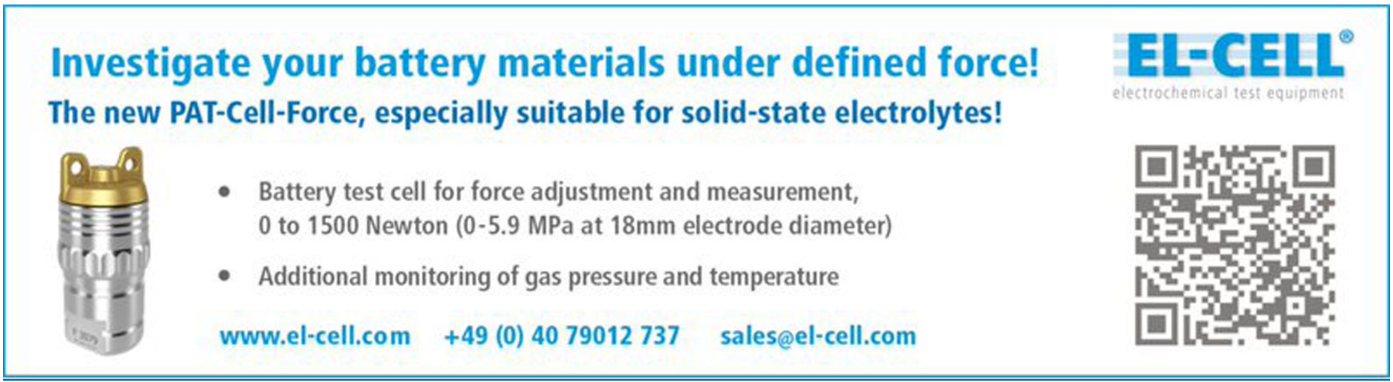

Sandia National Laboratories is a multimission laboratory managed and operated by National Technology & Engineering Solutions of Sandia, LLC, a wholly owned subsidiary of Honeywell International Inc., for the U.S. Department of Energy's National Nuclear Security Administration under contract DE-NA0003525.

ECS Journal of Solid State Science and Technology, 2022 **11** 063006

Surface Functionalized Barium Titanate Nanoparticles: A Combined Experimental and Computational Study

Jessica N. Domrzalski,[1] Tyler E. Stevens,[1] Renee M. Van Ginhoven,[2] Keith J. Fritzsching,[1] Brennan J. Walder,[1] Emily M. Johnson,[1,a] Riley E. Lewis,[1,b] Erika C. Vreeland,[1] Charles J. Pearce,[1] David A. Vargas,[1,c] Eric N. Coker,[1] Estevan J. Martinez,[1] John K. Grey,[1] and Todd C. Monson[1,z]

[1] *Sandia National Laboratories, Albuquerque, New Mexico 87185, United States of America*
[2] *Air Force Research Laboratory, Albuquerque, New Mexico 87117, United States of America*

Barium titanate (BTO) nanoparticles show great potential for use in electrostatic capacitors with high energy density. This includes both polymer composite and sintered capacitors. However, questions about the nanoparticles' size distribution, amount of agglomeration, and surface ligand effect on performance properties remain. Reducing particle agglomeration is a crucial step to understanding the properties of nanoscale particles, as agglomeration has significant effects on the composite dielectric constant. BTO surface functionalization using phosphonic acids is known reduce BTO nanoparticle agglomeration. We explore solution synthesized 10 nm BTO particles with *tert*-butylphosphonic acid ligands. Recent methods to quantifying agglomeration using an epoxy matrix before imaging shows that *tert*-butylphosphonic acid ligands reduce BTO agglomeration by 33%. Thermometric, spectroscopic, and computational methods provide confirmation of ligand binding and provide evidence of multiple ligand binding modes on the BTO particle surface.

[DOI: 10.1149/2162-8777/ac6f7d]

Manuscript submitted January 30, 2022; revised manuscript received May 3, 2022. Published June 6, 2022. *This paper is part of the JSS Focus Issue on Advances in Energy, Electronic and Dielectric Materials Development: From Methods to Applications.*

Supplementary material for this article is available online

Barium titanate (BTO) has excellent ferroelectric properties and a high dielectric constant; it therefore finds considerable use in devices, especially electrostatic capacitors.[1,2] This includes both polymer composite and sintered capacitors. While these benefits contribute to the widespread use of BTO, further study is necessary to better understand the properties of nanoscale BTO. In ceramics prepared with small (<1 μm) BTO particles there is some discrepancy between the predicted dielectric constant and the measured dielectric constant.[3–7] Dielectric constant is expected to decrease with grain size. However, the existence of a critical grain size below which ferroelectricity is lost and the exact value of such a critical size for BTO particles is debated.[4–7] The high frequency dielectric constant has been shown to increase with decreasing grain size until ca. 200 nm.[4] Nanocrystalline grain size also provides high breakdown strength and decreased strain. Thus, it is of considerable interest to develop a more thorough understanding of the relationship between particle size and dielectric constant. This knowledge could aid in the development of both composite and sintered electrostatic capacitors with improved energy densities and tunable properties.

One of the challenges in determining this relationship has been the tendency for BTO nanoparticles to form agglomerates. Phosphonic acids have been used to aid in the dispersion of metal oxide nanoparticles (including BTO) in organic solvents.[8,9] Phosphonic acid ligands have also proven to be effective when forming nanocomposites.[10,11] The effect of phosphonic acid ligands on dielectric constant has also been studied.[10,12] We seek to further improve BTO nanoparticles' stability in organic solvents using sterically bulky phosphonic acid ligands. Due to the highly tunable nature of these ligands, such as alkyl chain length and functionality, this method allows for a study of different ligand moieties and their surface interactions. Furthermore, functionalization of the non-binding end of the phosphonic acid could allow for direct incorporation of the particles into an epoxy system to form a matrix-free composite.[13] This would enable subsequent extraction of reliable dielectric information for discrete nanoparticles.

The tendency of nanoscale particles to agglomerate is a common and challenging problem to confront. This agglomeration tendency must also be avoided during characterization steps. To avoid solvent drying artifacts in our imaging studies, we generated epoxy-based composites. Extracting more detailed information regarding the size of the of particles and agglomeration is expected to be an important step towards further investigation on dielectric constant.

Here, a solution-based synthesis, which allows for less agglomeration, more facile surface functionalization, and avoids some of the challenges inherent to other methods, was chosen to synthesize the BTO particles. We report the functionalization of BTO and incorporation of these particles into an epoxy composite. Spectroscopy, thermogravimetry, and density functional theory (DFT) calculations show that the BTO surface is modified with ligands, including hydroxides, water, ethanol, and *tert*-butylphosphonic acid in multiple binding modes.

Experimental

All manipulations were performed using standard Schlenk techniques. Ethanol, purchased from Pharmco, was degassed, and stored over 3 Å molecular sieves. All other reagents were purchased from Sigma-Aldrich and used as received. 10 nm BTO particles were synthesized according to a published procedure.[14] The use of Schlenk techniques minimized the formation of barium carbonate. Particle size was controlled by measured water addition using a peristaltic pump. 60 molar equivalents of water were added at a rate of 4 ml min^{-1}.

The BTO (10 nm) nanoparticles were functionalized with *tert*-butylphosphonic acid (tBuPA). 30 ml of a 0.0286 M solution of ligand in toluene was added to a 50 ml three-neck round bottom flask fitted with a condenser and heated while stirring to 115 °C. Once at reflux, isolated BTO nanoparticles (0.858 mmol, 0.2 g) suspended in

---

[a] Present Address: E.M.J. Missouri S&T, Department of Explosives Engineering, Rolla, Missouri 65409, United States.
[b] Present Address: R.E.L. University of Minnesota, Department of Chemistry, Minneapolis, Minnesota 55455, United States.
[c] Present Address: D.A.V. University of New Mexico, Department of Mathematics & Statistics, Albuquerque, New Mexico 87131, United States.
[z] E-mail: tmonson@sandia.gov

5 ml absolute ethanol were added dropwise to the ligand solution and stirred with heat for 15 min. The mixture was sonicated for 30 min and returned to stirring at reflux for two hours. The modified nanoparticles were separated by centrifugation and washed with toluene (3 × 10 ml) to remove excess ligand. The particles were dried in vacuo at 60 °C for 24 h. If the particles were to be used for composite fabrication, they were resuspended in ethanol.

Both functionalized and unfunctionalized BTO particles were used to form epoxy composites for further study. These composites were fabricated with a 1:0.75 molar ratio of trimethylolpropane triglycidyl ether:4-aminophenlysulfone. The BTO particles were added based upon desired volume percent. Trimethylolpropane triglycidyl ether was added to the particles and vortexed until fully mixed. If clumps still existed at higher volume loadings, the solution was left on a stir plate for 24 h. 4-aminophenyl sulfone was added to the solution and mixed further at 100 °C until fully incorporated. This final mixture was transferred from the vial to a silicone mold that was coated with Apiezon H grease. The mold was placed in a vacuum chamber on a hot plate at 150 °C. Vacuum was applied until bubbling stopped. The mold was left on the hot plate at 185 °C for 24 h to complete the cure.

Various techniques were used to characterize the particles and the composites to better understand how the ligands affect the properties of BTO. Fourier transform infrared (FTIR) spectra were obtained on a Bruker IFS 66/S using KBr pellets containing 1% wt of sample. Thermogravimetric analysis (TGA) was performed on a Netzsch STA 499 F1 Jupiter in alumina crucibles with a ramp rate of 15 K $\min^{-1}$. Dynamic light scattering (DLS) measurements were performed in ethanol using a Malvern Zetasizer Nano ZS. Epoxy samples were prepared for transmission electron microscopy (TEM) analysis via a Leica EM UC7 Ultramicrotome. TEM micrographs were acquired on a JEOL JEM 1200EX or a Tecnai F30. Solid-state NMR experiments were performed on a Bruker (Billerica, MA) Avance II spectrometer. The experiment operated at a resonance frequency of 600 MHz for ^{1}H using a 2.5 mm HX or HXY magic-angle spinning (MAS) probe. The MAS frequency was set to 27.777 kHz unless otherwise noted. Typical ^{1}H, ^{13}C, ^{31}P 90° pulse lengths were 2.4, 3.4 and 3 μs, respectively. ^{13}C (^{1}H) Cross-polarization (CP) experiments were performed with a typical contact time of 2 ms and close to 100 kHz radio-field strengths for ^{1}H channel and a recycle delay of 1 s. ^{31}P (^{1}H) Cross-polarization (CP) experiments were performed with a typical contact time of 2.5 ms and close to 100 kHz radio-field strengths for ^{1}H channel and a recycle delay of 2.5 s. ^{13}C shifts were externally referenced to the most up-field adamantane peak to 34.48 ppm on the trimethylsilane scale. ^{31}P shifts were externally referenced by setting ammonium phosphate monobasic to 0.8 ppm on the 85% phosphoric acid scale. ^{1}H shifts were referenced indirectly, using the gyromagnetic ratios and the ^{13}C reference.

The effect of tBuPA stereochemistry on NMR chemical shifts was determined by electronic structure calculation. Models of tBuPA were geometry optimized by DFT using the B3LYP functional in Gaussian16 (Gaussian Inc., Wallingford, CT), with the O=P–C–C dihedral angle frozen to 0° (eclipsed) or 180° (staggered) during the optimization. Magnetic shielding tensors for all nuclei were calculated using the gauge-including atomic orbital method. The 6–311++G(d,p) basis set was chosen for these calculations as this set has been shown to provide accurate and computationally affordable results when used for NMR calculations of nucleic acid phosphate systems.[15,16] The chemical shielding values were converted to shift values using a previously published relation:[15–17]

$$\delta_{\text{calc}}(^{31}\text{P}) = -266.1\ \text{ppm} + \sigma_{\text{calc}}(^{31}\text{P, PH}_3) - \sigma_{\text{cal}}(^{31}\text{P}) \qquad [1]$$

The likely binding modes of tBuPA onto BTO particles were investigated with DFT as implemented in the SEQQUEST code.[18] We used the generalized gradient functional as formulated by Perdew, Burke and Ernzerhof (PBE).[19] Optimized norm-conserving pseudopotentials were used for all atoms.[20] With PBE, the lattice parameters are slightly larger than experiment, the material is softer (has lower elastic constants), and the *c*/*a* ratio and internal displacements are therefore slightly exaggerated.[14] However, we expect surface relaxation, chemistry, and particularly weakly bound surface treatments to be better described by PBE. We constructed a 4 × 4 × 4 slab from the optimized cubic paraelectric unit cell, with both surfaces terminated with BaO (352 total atoms). The slab was fully relaxed to a tolerance of 0.04 eV/Å. The bare slab was compressed slightly in *z* and remained paraelectric. Except where stated otherwise, all tBuPA binding calculations discussed in this work use this slab.

Results and Discussion

We found that by using a modified procedure,[20] rather than the method of Yoon et al.,[21] we were able to consistently form particles of desired sizes. To limit BTO nanoparticle agglomeration, we performed a ligand exchange reaction to replace the surface alkoxide and hydroxide ligands with phosphonic acid ligands. We hypothesized that modifying the surface of the particles with bulky alkyl phosphonic acid ligands to form a protective shell would inhibit agglomeration (Fig. 1).[22]

The as-functionalized particles were isolated and characterized by TEM (Fig. 2), FTIR (Fig. 3), TGA (Fig. 4), and solid-state NMR (Fig. 5). DLS was used to analyze the size distribution of the functionalized particles in solution. Because we suspected that the functionalization would not change particle size, but reduce particle agglomeration, DLS was used to confirm smaller agglomerates upon addition of the phosphonic acid ligand but detailed DLS analysis was not pursued. This data can be found in the supplementary

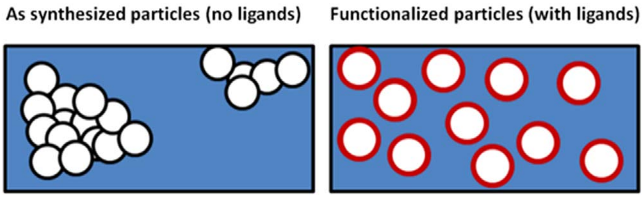

Figure 1. Depiction of unfunctionalized BTO nanoparticles in the left image and functionalized BTO in the right image. This image is an idealized depiction for multiple media including solution and polymer-based composites.

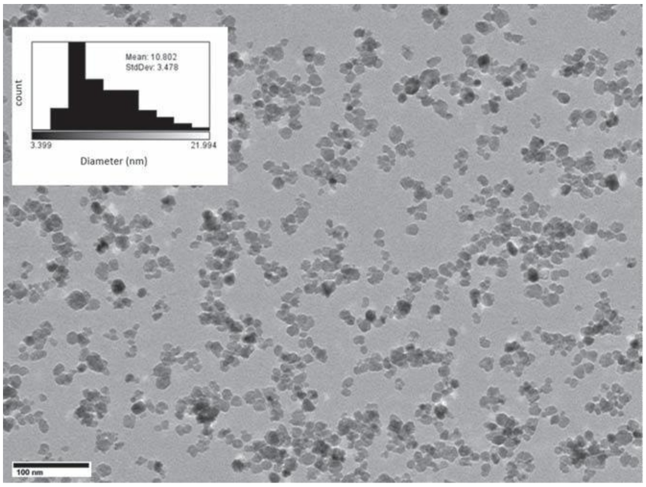

Figure 2. TEM micrograph of (tBuPA)BTO. The inset shows the mean particle diameter to be 10.802 ± 3.478 nm.

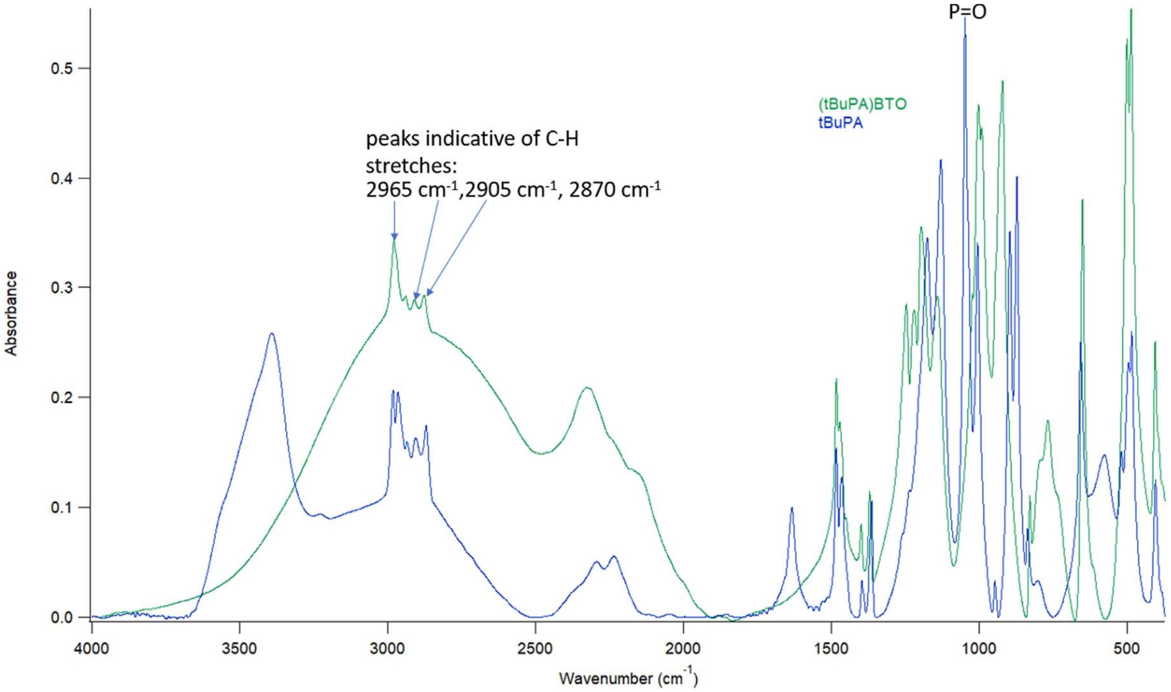

Figure 3. FTIR spectra of free ligand is shown in blue and functionalized (tBuPA)BTO particles in green.

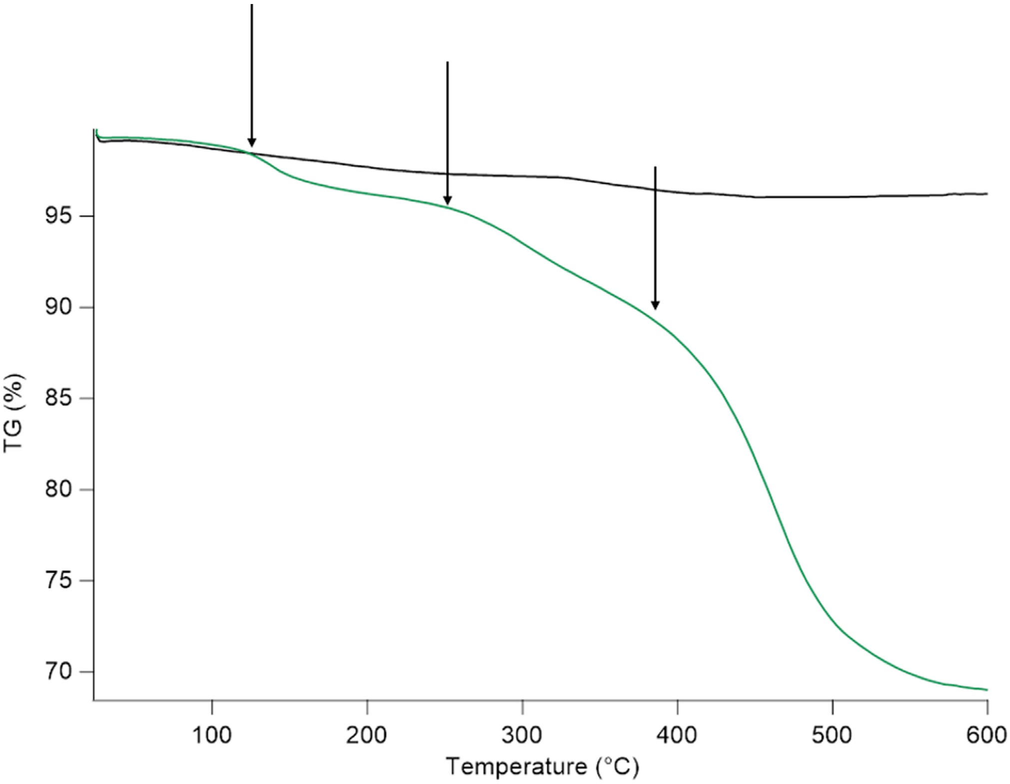

Figure 4. TGA traces for BTO (black), and (tBuPA)BTO (green) Arrows show the beginning of mass loss.

information, Fig. S1 (available online at stacks.iop.org/JSS/11/063006/mmedia).

The FTIR data is consistent with a successful functionalization of the BTO surface. C–H stretches at 2965, 2905, and 2870 cm^{-1} for (tBuPA)BTO indicate the presence of the ligand.[23] Furthermore, the stretching frequencies corresponding to the P=O bond centered around 1200 cm^{-1} are significantly shifted upon functionalization of the BTO particles as shown in Fig. 3. More FTIR data, including data of particles functionalized with aminopropyl phosphonic acid, and neat BTO, can be found in Figs. S6 and S7 in the supplementary information.

To further confirm that the BTO particles had successfully been functionalized, TGA was performed. Notably, the branched (tBuPA) alkyl phosphonic acid modified BTO particles showed a marked

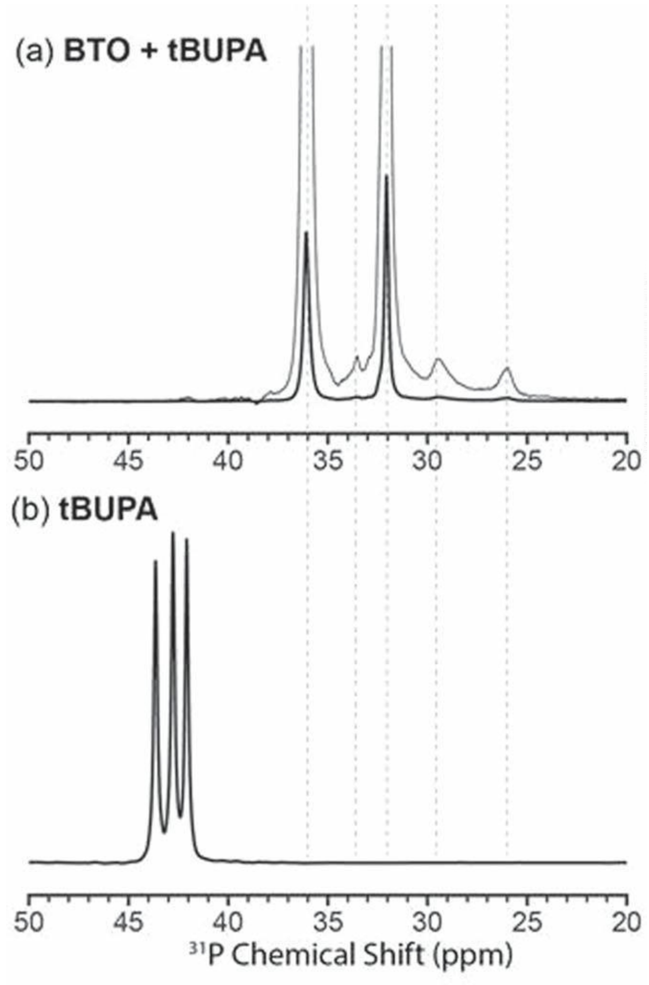

Figure 5 : Solid-state NMR ^{31}P(^{1}H) CP spectra of BTO with tBuPA (a), and tBuPA starting material(b). The thick spectra are scaled so that their noise levels are the same, the thin spectrum is the same but scaled by 10 to highlight the smaller peaks.

difference to the unfunctionalized BTO particles, experiencing a mass loss of 31%. Further, the (tBuPA)BTO experienced the onset of mass loss at approximately 130 °C followed by two more stages of mass loss at higher temperatures (Fig. 4). Further TGA-mass spectrometry (MS) data can be found in the supplementary information, Fig. S5.

The first stage of TGA mass loss near 130 °C corresponds to the removal of residual bound water, as supported by our TGA-MS data. One possible explanation for the latter two stages of TGA mass loss is that the bulky tBuPA ligand binds to the surface in different modes, (i.e., monodentate, bidentate, or tridentate) as these have different binding energies.[23] These binding modes have been observed for organophosphorus moieties binding to related metal oxides.[24] One could envision that if three tBuPA ligands are close in proximity, there may be sufficient steric bulk that the two adjacent ligands can only bind through one or two of the oxygen moieties. In this case, the energy required for dissociation of these ligands is expected to be lower, resulting in a separate stage of mass loss at a lower temperature.

To explore the different binding modes on a molecular level, solid-state NMR was performed. The ^{31}P solid-state NMR spectra of tBuPA in pure crystalline form and bound to the BTO particles is shown in Fig. 5. Crystalline tBuPA acid yields three approximately equally intense peaks with chemical shifts $\delta_P =$ 42.1, 42.7 and 43.6 ppm. The crystal structure of tBuPA (CCDC: 183676) has three molecules in the unit cell; the three peaks in the ^{31}P spectra are attributed to these three sites.[25] The chemical shift difference in the crystal is either due to local hydrogen binding or changes in the configuration of the molecules. We calculated the expected chemical shifts of tBuPA in two different configurations, where the *t*-butyl group is eclipsed or staggered with respect to the $PO(OH)_2$ group (i.e., the $P\text{-}C(CH_3)_3$ bond is rotated) using electronic structure calculations. The eclipsed configuration gave $\delta_{calc}(^{31}P) =$ 45.2 ppm, and the staggered configuration gave $\delta_{calc}(^{31}P) =$ 44.4 ppm. We note that difference, $\Delta\delta_{calc}(^{31}P) = 0.8$ ppm, is close to the difference between the experimental peaks ($\Delta\delta_{expt}(^{31}P) = -0.6, +0.9$ ppm from the center peak).

The ^{31}P spectrum (Fig. 5a) of the ligand bound to the BTO particles show two intense peaks at 36.1 ppm and 32.1 ppm and two minor species at 29.5 and 26.1 ppm. All these peaks are substantially shifted from the free ligand signals, clearly showing that the ligand is bound to the BTO particles. Additionally, the BTO bound spectra show no ^{31}P peaks near 43 ppm, demonstrating that any non-bound ligand was successfully removed during the washing protocol. The $\Delta\delta_{expt}(^{31}P)$ calculated for configuration changes in the free ligand (0.8 ppm) is much smaller than the experimental shift differences observed for the bound ligands ($\Delta\delta_{expt}(^{31}P) > 3.5$ ppm, between all peaks). Therefore, we dismiss the possibility that the multiple ^{31}P sites in the bound ligand are only due to different internal configurations. Variable contact time 2D ^{31}P-^{1}H HETCOR NMR (Fig. S2) and further DFT simulations illustrate that the different resolved chemical sites are the result of different protonation states and binding configurations of the ligand to the BTO particles. The HETCOR experiments show that the phosphorus site at $\delta(^{31}P) =$ 36.1 ppm is spatially closest to –OH groups resonating at $\delta(^{1}H)=$ 9.8 ppm, while the $\delta(^{31}P) =$ 32.1 ppm site is closer to the $\delta(^{1}H)=$ 10.5 ppm –OH groups. The two minor species at $\delta(^{31}P)=$ 29.5 and 26.1 ppm are not correlated to any –OH signal but instead are correlated to a minor peak near $\delta(^{1}H)=$ 16.5 ppm. A proton chemical shift of 16.5 ppm is characteristic of a ^{1}H shift in a O–H··O hydrogen bond. We speculate that this hydrogen bond forms when the ligand hydrogen bonds to –OH groups that decorate the surface before tBuPA functionalization (see solid-state ^{1}H NMR spectra, Fig. S3).[26] The solid-state ^{13}C NMR spectra (Fig. S4) are consistent with the other NMR data.

In addition to characterizing their chemical structure, the particles were incorporated into epoxy composites to measure agglomeration behavior. Often, agglomeration is quantified by depositing an aliquot of the suspension on a TEM grid and analyzing micrographs. To avoid undesirable drying effects, our approach was to incorporate the BTO particles into an epoxy matrix at different volume loadings and subsequently microtome the resulting composites for TEM analysis. Kaufman et al. defined the degree of agglomeration as $f_a = (N_a n^3)/N_p$.[27] Here, f_a is the degree of agglomeration, N_a is the total number of agglomerates, n is the number of particles along the edge of a perfectly cubic agglomerate, and N_p is the total number of particles, agglomerated or not. The cubed n term suggests a cubic arrangement for agglomerates in 3D space, a restriction that is not relevant here. Thus, we define a BTO agglomerate as comprising four or more particles stuck together, with an area of 314.59 nm^2 or larger and assume the particles are circular and of uniform size of ~78.6 nm^2. Two and three particle clusters do not constitute an agglomerate. The following equation was used to assess degree of agglomeration:

$$f_a = (N_a n)/N_p \qquad [2]$$

Each degree of agglomeration analysis was made for a single TEM of varying area. Several micrographs from the same batch were needed to generalize each analysis to a sample of BTO. It should be noted that several images were examined to come up with the summarized results in Table I. Not all of these are included here,

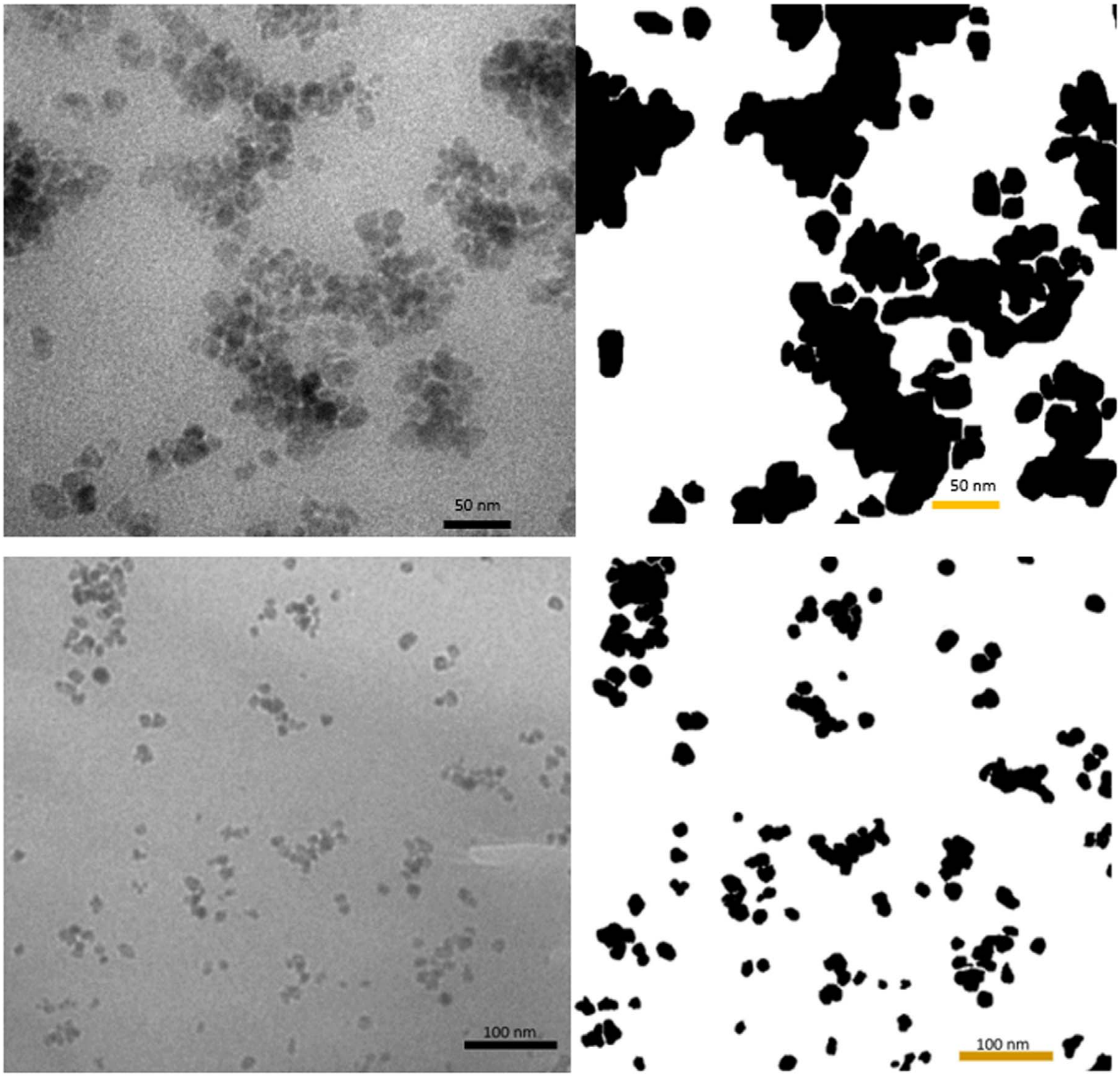

Figure 6. Micrographs before and after ImageJ processing of epoxy containing 10 vol% unfunctionalized BTO particles (top) and 10 vol% tBuPA functionalized BTO particles (bottom). Imaged on a JEOL JEM 1200EX.

for succinctness. Three micrographs each were analyzed from these particular batches of functionalized and unfunctionalized particles, totaling an area of 1,925,510 square nanometers comprising of more than 1,000 particles. To conduct this analysis, ImageJ software was utilized. The desired portion of an image was duplicated after the scale was applied. Then, the despeckle function was used to reduce noise, which easily skews edge detection results because each pixel is wrongly assumed as an edge. When a simple brightness/contrast adjustment was not successful, a Gaussian filter was convolved with the image, which further reduces noise and lessens detail. This is important when fine detail is not necessary because the edges become the focal point of the image. To analyze the particles with these filters applied, the image must be converted to a binary image rather than a grayscale image. This allows each pixel to be represented as a 0 or a 1 rather than a range from 0 to 256. The edges were found using the "find edges" function. If the image was still too grainy after multiple despeckling attempts, the edges were manually traced, and the image smoothed. Next, a threshold was applied with a dark background. The threshold values vary greatly from image to image due to differences in TEM set-up, magnification used, sample thickness, and general image quality. Any pixels that the threshold failed to eliminate were painted over by hand, and any holes that were not filled were filled using the flood tool. To arrive at the final values needed for calculation, the particles were analyzed by the software and then sorted by size.

The as mentioned epoxy composites were prepared using 10 vol% BTO (Fig. 6, top) and 10 vol% (tBuPA)BTO (Fig. 6, bottom). Micrographs of the described particles in epoxy with areas 95,208 nm^2 and 277,224 nm^2, respectively, were analyzed using ImageJ software.

The calculated degree of agglomeration of the unfunctionalized particles is 86.8%. The left image is untouched, and only cropped from the original TEM, while the right image is the product of the processing steps listed above. Similarly, BTO functionalized particles have a degree of agglomeration of 68.9%.

Notably, analysis of the micrographs show that agglomeration was reduced in the sample containing the functionalized (tBuPA) BTO nanoparticles. Upon processing the TEMs and applying Eq. 2, the calculated degree of agglomeration was reduced by an average of 33.3% (Table I). Although the agglomeration was not reduced to zero, this difference moves us closer to elucidating nanoscale properties of discrete nanoparticles.

The interaction of the molecular species used in the synthesis, functionalization, and suspension of the BTO particles in solution was investigated using DFT. Specifically, the interaction of the tBuPA ligand, as well as H_2 and H_2O, with the fully relaxed 4 × 4 × 4 BaO terminated BTO slab (Fig. 7) was examined.

Table I. Calculated degree of agglomeration from TEMs.

Sample area analyzed (nm^2)	Degree of agglomeration	Average degree of agglomeration
10 vol% BTO particles in epoxy		92.9% ± 5.5%
311242	0.976	
95208	0.868	
1059300	0.943	
10 vol% (tBuPA)BTO particles in epoxy		59.6% ± 8.6%
88592	0.579	
277224	0.689	
93944	0.520	

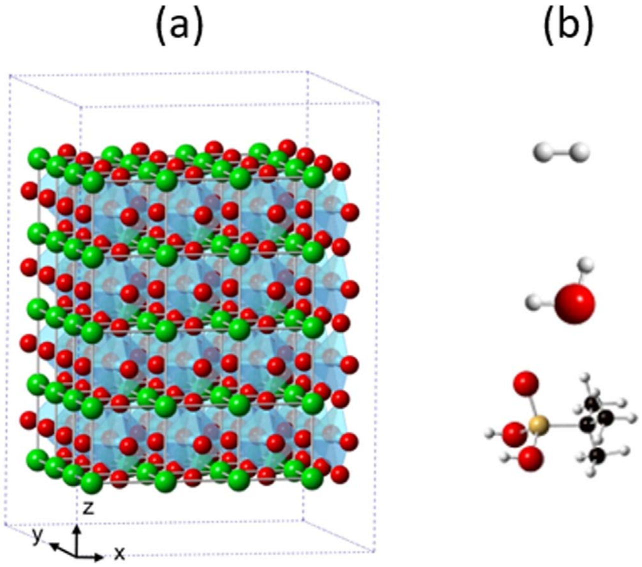

Figure 7. (a) $BaTiO_3$ supercell slab used in the surface reaction calculations. The system is periodic in the *xy*-plane. On the right, (b) is the selected set of molecules examined in the surface reaction calculation set. Ba is green, O is red, and Ti is pale blue. C is black, P is yellow, and H is white.

Table II. Interaction energy for water and BTO slab.

H_2O molecule placement	Energy relative to infinite separation (eV)
5 Å separation	−1.09
Adsorbed at surface	−1.79

Table III. Constrained Relaxation of Surface Hydrogen.

Relaxation	H atom binding energy (eV)
Top layer only	0.76
Top two layers	0.01
Top three layers	−0.19
Top half of slab	−0.83
Full slab	−1.07

There are multiple challenges inherent in the atomistic simulation of ferroelectric systems. First, there is a large polarization response that increases the difficulty of surface chemistry calculations. The binding energy of a surface adsorbent is calculated as

$$E_{bind} = E_{(relaxed\ slab+molecule)} - E_{slab} - E_{molecule} \quad [3]$$

In general, the introduction of a molecule with a dipole moment may be expected to induce a polarization response in a slab. For a non-ferroelectric material, this polarization is a minor contribution to the system energy problem and can be simply rolled into the interaction or binding energy. For a ferroelectric system such as BTO, we find that the polarization response may be on the order of or even larger than a typical binding energy. In order to adequately investigate surface chemistry, it is necessary to deconvolute the energetics of longer-range polarization response from surface reactions. Second, a slab of ferroelectric material can exhibit a multitude of complex domain behaviors[14] with numerous possible transitions into different ferroelectric phases and collections of domains, each of which has a different polar interaction with any added atoms or molecules.[28–30] Finally, the forces involved in the system polarization and domain formation are small on a per atom basis, requiring tight force convergence criteria and long relaxation times.

The consequence of the slab polarization response is seen immediately when calculating the adsorption of a water molecule on the paraelectric slab surface. In Table II, we show the results for full relaxation of the molecule and slab held at a 5 Å separation, and with the water molecule adsorbed at the surface. There is significant polarization response evident in the calculated binding energies, which are higher than might be expected from simple physisorption, even at considerable distance. For example, the binding energy of H_2O on the (001) surface of anatase TiO_2 has been reported to be from 0.48 eV to 0.82 eV. For $SrTiO_3$ surfaces, the binding energy of H_2O has been reported as 0.8 eV for SrO termination, and 0.74 eV for TiO_2 termination. Therefore, for BTO, we see that addition of the ferroelectric polarization response results in a binding energy of H_2O that is likely about double the expected value. The magnitude of the binding we calculate, 1.8 eV, is on the same order as covalent bonding.

As may be expected, the interaction of a hydrogen atom with the BTO surface is also significantly affected by the polarization response. In this case, we examined the effect of allowing relaxation of different numbers of slab layers on the calculated binding energy for a single hydrogen atom bound to a slab surface oxygen atom.

The binding energy is calculated relative to the pristine paraelectric slab and the hydrogen molecule as:

$$E_{rxn} = E_{(slab+H)} - E_{slab} - (1/2)E_{H_2} \quad [4]$$

Table III shows the results for the H atom binding energy with relaxation constrained to the first BaO surface layer, the first two layers (BaO and TiO_2), 3 layers (Bao/TiO_2/BaO), half the slab thickness, and allowed for the full slab. As the number of layers relaxed increases, the binding energy changes dramatically, from strongly endothermic to strongly exothermic compared to H_2 at infinite distance.

The polarized (ferroelectric) response can also be seen directly by examining the atomic configuration. The atom positions for the slab + H configuration are shown in Fig. 8. There is significant surface distortion, with the oxygen bound to the hydrogen pulled upward, and the titanium atoms in the column below pushed downward. With full relaxation, this distortion propagates though the full slab thickness.

Study of surface chemistry in a ferroelectric material is also affected by the complex possible arrangements of domains and polarization prior to adsorption or reaction at the surface. In

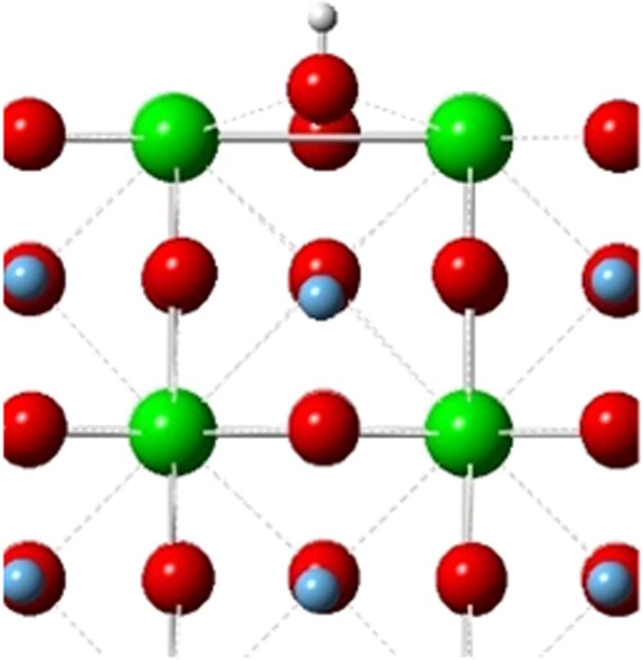

Figure 8. Binding of a hydrogen atom to a surface layer oxygen atom in the BTO. The hydrogenated oxygen rumples upward, and the Ti atoms in the column underneath rumple away from the surface.

examining the phase and polarization behavior of bare BTO slabs, we find that in a slab geometry, the system tended to find the paraelectric phase unless an initial distortion toward a ferroelectric configuration was imposed as a starting condition, even when the ferroelectric minimum is lower in energy. This indicates that the effective capture basin for the paraelectric phase is relatively wide, so that initial conditions over conventionally chosen phase space will tend to that minimum. However, with the addition of a perturbation, such as thermal energy, applied fields, or a polar molecule or defect, the system may overcome the barrier into the narrower but lower minimum. Previous work, both our own, and as reported multiple times in the literature, shows that for a slab (thin film or wire) configuration, the boundary conditions dictate that the net polarization of the system in non-periodic directions must sum to zero.[31] Ferroelectricity in the non-periodic directions may be enabled by screening, such that the polarization is compensated by the screening material, by sets of multiple domains with opposing polarization, or by the construction of polar surfaces. Polarization in the periodic directions is not limited in this way, as the conditions in standard formulation for periodic calculations result in non-polar boundaries at infinity.

We performed a limited set of calculations on bare ferroelectric slabs to examine relevant phase energetics (Fig. 9, Table IV). The construction and relaxation of an opposed 2-domain ferroelectric phase (one up and one down in Z) lowers the slab total energy by 0.013 eV per $BaTiO_3$ unit cell. At the slab size required to describe surface chemistry, this results in a total system relaxation of nearly 1 eV. This value may also be expected to change with the system size, as there is an energetic cost to the formation of domain walls. Construction of a tetragonal ferroelectric slab with the polarization parallel to one of the periodic cell vectors (tetragonal phase oriented in the x or y direction), also results in a significantly lower overall energy (0.010 eV per unit cell, for a total of −0.67 eV for the slab). This result means that for this system, we expect to see an energy difference in the range of 0.7 to 1 eV solely due to changes in the material polarization, in addition to the effect of any bonds formed at the surface.

Finally, the optimization of the geometry involves a large set of small relaxations of atomic motions along shallow potential energy surfaces. Without acceleration techniques, this requires many iterations, driving up overall computational costs.

To meaningfully investigate surface chemistry, it is necessary to deconvolute the energetics of longer-range polarization response from surface reactions. There are multiple possible approaches, including using one of the ferroelectric slabs constructed here. Unfortunately, these ferroelectric slabs introduce additional issues, and potentially prohibitive computational expense. For example, the 2-domain slab requires construction of a much larger slab to provide

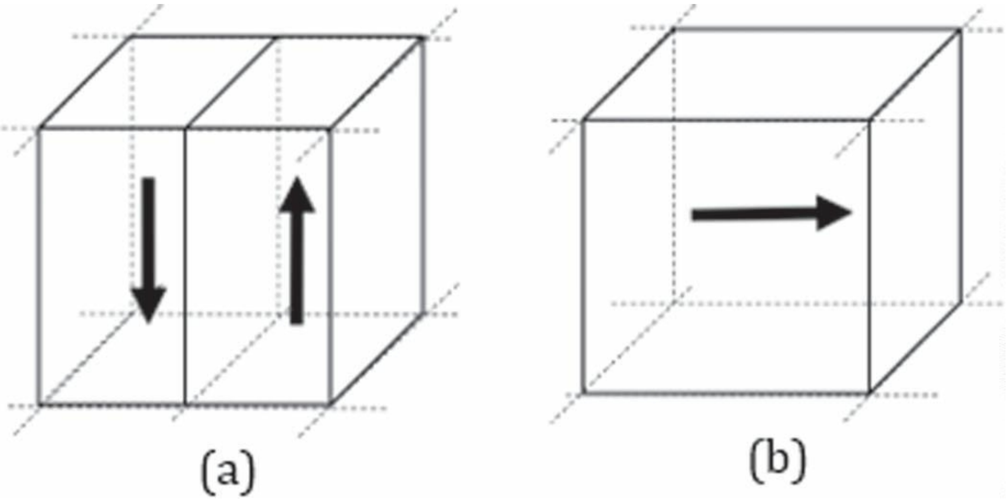

Figure 9. Conceptual illustration of two possible ferroelectric domain arrangements in the slab configuration. The system is periodic in the *xy*-plane. (a) Two opposing polarized domains of equal size in +*z* and –*z*. (b) A single ferroelectric polarization parallel with the periodic plane. (In this case,the *xy*-plane.)

Table IV. Paraelectric vs ferroelectric slabs.

Description of ferroelectric slab structure	Normalized energy relative to paraelectric slab (eV)
2-domain opposed in Z	−0.82
1-domain Tetragonal in Y	−0.67

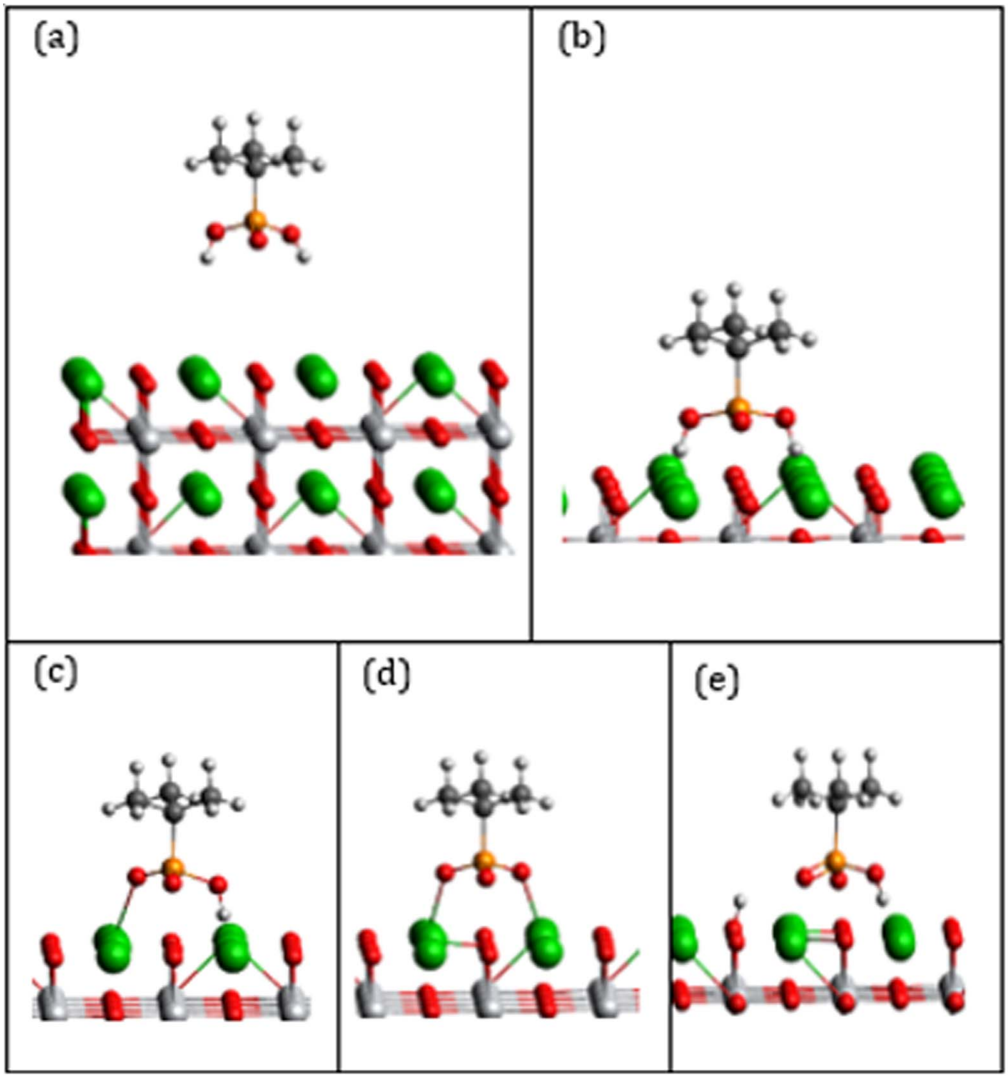

Figure 10. tBuPA on the BaO-terminated surface of BTO. Each possible configuration of absorbed and dissociated acid is considered. Ba is green, oxygen is red, and Ti is pale blue. Carbon is back, phosphorus is yellow, and hydrogen is white. Configuration (e) is the lowest energy. The relative energy for each configuration is shown in Table V.

a domain surface of sufficient size for reactions with the ligand molecule while avoiding the domain wall. We estimate 5 to 6 unit cells will be needed per domain, leading to a slab size in the range of 1,000 atoms, near the limit for many DFT codes. There are also additional complications due to interactions near domain walls, and the approach does not account for further induction of in-plane polarization. The in-plane polarized slab produces preferred orientations for molecules and does not resolve the perpendicular polarization that would still occur. For the present work, instead of these more complicated and computationally intensive approaches, we chose to use a constrained optimization method.

The calculations of surface chemistry were simplified by performing optimizations with only the top three layers of the slab free to respond. This eliminates most of the polarization response and enables the calculation of relative energetics and reaction mechanisms. This approach is necessarily a compromise but should capture some of the desired chemistry. We determined the optimum number of layers to relax through examination of the hydrogen atom bonding calculations detailed above.

Relaxing only the top one or two layers leads to repulsion or negligent bond energy and may be considered inadequate to describe surface binding. Relaxing the top three atomic layers of the slab allows for reasonable bonding energy for H to the surface, while suppressing most of the polarization.

Using the results for the top three relaxation, we find that hydrogen will tend to dissociate at the surface and bind to oxygen. It is possible to find a local minimum in which the H atom is bound to a Ba surface atom through restricting the symmetry of the relaxation. However, this site is significantly higher in energy at all levels of relaxation, and any off-center placement resulted in a spontaneous hop to an oxygen site.

The interaction of tBuPA with the BaO-terminated slab surface was examined using the constrained 3-layer slab relaxation. The results are shown in Table V, and the corresponding configurations are shown in Fig. 10. Formation energy of the acid + BTO surface is calculated in the following ways. For ligand binding:

$$E_{rxn} = E_{(slab+acid)} - (E_{slab} + E_{acid}) \tag{5}$$

For single H dissociation:

$$E_{rxn} = (E_{(slab+acid-H)} + E_{(slab+H)}) - (2E_{slab} + E_{acid}) \tag{6}$$

And for double H dissociation:

$$E_{rxn} = (E_{(slab+acid-2H)} + 2E_{(slab+H)}) - (3E_{slab} + E_{acid}) \tag{7}$$

Each possible bonding arrangement with and without dissociated hydrogen atoms is a local minimum. As with previous calculations

Table V. Binding energy of acid ligand to BaO surface. The lettering corresponds to Fig. 10.

Configuration	E_{rxn} eV (relative to gas phase acid and adsorbed H)
(a) tBuPA at 5 Å	−0.03
(b) tBuPA at surface	−3.17
(c) 1 diss. H (inf)	−1.55
(d) 2 diss. H (inf)	0.25
(e) 1 near diss. H	−3.42

of phosphonic acids on the BaO surface, the lowest energy position of the ligand is with the central phosphorus atom above a surface oxygen, and the oxygens in approximately the position of the next layer of oxygens expected for the sequential crystal layer. Each of the configuration types explored has multiple local minima, within a range of less than 0.1 eV. We report the lowest energy result for each configuration type. For the whole, undissociated molecule at a distance of 5 Å, there is a minor distant response of the surface, indicating that the 3-layer relaxation allows for a response, but not large-scale polarization (the ligand does have a dipole in the *xy*-plane in the orientation shown). The two dissociated configurations assume that the removed hydrogen atom is also attached to the BTO surface, at a distance sufficient to avoid interacting with the molecule. It is immediately apparent that these configurations are not favorable compared to the undissociated molecule. The lowest arrangements found are what we have termed near-dissociated, as shown in Fig. 10e, wherein one of the hydrogen atoms is bound to a surface oxygen adjacent to the molecule, displaying significant interaction between this surface-bound atom and the molecule. There are at least four of these arrangements, all within 0.1 eV in energy. The results are similar both in energetics, and in the general nature of the geometric arrangements of the acid-ligand binding, to the reported calculated results for phosphonic acid adsorbed on the planar anatase TiO_2 surface in Geldof.[21]

To connect with the thermal desorption experiments, we performed calculations of the reaction pathways of the removal processes for the energetically favorable configurations. The results show that while there are local barriers for configurations with nearby dissociated hydrogen atoms, the overall desorption barrier is essentially the same as the binding energy. These are rather high barriers, and we acknowledge that this approach leads to results that provide only limited correlation with the experiments. There are several factors that the work does not consider, including interaction with different surface terminations (TiO_2 or mixed phases), the fully saturated surface termination with hydrogen and hydroxyl groups before the introduction of the acid ligand, and consideration of solvation effects. Solvation effects are beyond the scope of this type of DFT calculation, but the pre-saturated surface and different surface terminations will be considered in future work. Solvation and thermal effects may be more effectively included through molecular dynamic simulations with use of an appropriate reactive interatomic potential.

Conclusions

We have shown that it is possible to reduce BTO nanoparticles' agglomeration by 33% in epoxy composites using a phosphonic acid ligand to modify the surface. Calculations show binding is possible through all three oxygen moieties, although it is expected that other binding modes are also observed due to the sterically demanding *tert*-butyl moiety. Implementing the functionalized particles into an epoxy composite and comparing them to non-functionalized BTO particles in composites allowed us to quantify the extent to which agglomeration can be prevented in this system. This increase in surface passivation and subsequent decrease in agglomeration will aid in both the further study of discrete ferroelectric nanoparticles and the formation of improved dielectric composites for electrostatic capacitors. Additional experiments and future publications will describe ferroelectric responses according to the degree of particle agglomeration.

Acknowledgments

The authors thank Dr. Susan Heidger of the Air Force Research Laboratory/High Power Microwave Electromagnetic Microwave Division for significant support of this work. This work was performed, in part, at the Center for Integrated Nanotechnologies, an Office of Science User Facility operated for the U.S. Department of Energy (DOE) Office of Science. Sandia National Laboratories is a multi-mission laboratory managed and operated by National Technology and Engineering Solutions of Sandia, LLC., a wholly owned subsidiary of Honeywell International, Inc., for the U.S. DOE's National Nuclear Security Administration under contract DE-NA-0003525. The views expressed in the article do not necessarily represent the views of the U.S. DOE or the United States Government.

ORCID

Jessica N. Domrzalski https://orcid.org/0000-0002-2184-6123
Charles J. Pearce https://orcid.org/0000-0002-5497-640X
Eric N. Coker https://orcid.org/0000-0002-9382-9373
Todd C. Monson https://orcid.org/0000-0002-9782-7084

References

1. D.-H. Yoon, "Tetragonality of barium titanate powder for a ceramic capacitor application." *J. Ceramic Proc. Res.*, **7**, 343 (2006).
2. B. Ertuğ, "The overview of the electrical properties of barium titanate." *A.J.E.R.*, **2**, 1 (2013).
3. S. Wada, T. Hoshina, H. Kakemoto, and T. Tsurumi, "Preparation of nm-ordered barium titanate fine particles using the 2-step thermal decomposition of barium titanyl oxalate and their dielectric properties." *Proceedings of the 13th IEEE International Symposium on Applications of Ferroelectrics, 2002. ISAF 2002*263 (2002).
4. K.-L. Ying and T. E. Hsieh, "Sintering behaviors and dielectric properties of nanocrystalline barium titanate." *Materials Science and Engineering: B*, **138**, 241 (2007).
5. M. H. Frey, Z. Xu, P. Han, and D. A. Payne, "The role of interfaces on an apparent grain size effect on the dielectric properties for ferroelectric barium titanate ceramics." *Ferroelectrics*, **206**, 337 (1998).
6. S. M. Aygün, J. F. Ihlefeld, W. J. Borland, and J.-P. Maria, "Permittivity scaling in $Ba_{1-x}Sr_xTiO_3$ thin films and ceramics." *J. Appl. Phys.*, **109**, 034108 (2011).
7. T. Tunkasiri and G. Rujijanagul, "Dielectric strength of fine grained barium titanate ceramics." *J. Mater. Sci. Lett.*, **15**, 1767 (1996).
8. I. Maege, E. Jaehne, A. Henke, H.-J. P. Adler, C. Bram, C. Jung, and M. Stratmann, "Self-assembling adhesion promoters for corrosion resistant metal polymer interfaces." *Prog. Org. Coat.*, **34**, 1 (1998).
9. R. Pązik, R. Andersson, L. Kępiński, J.-M. Nedelec, V. G. Kessler, and G. A. Seisenbaeva, "Surface functionalization of the metal oxide nanoparticles with biologically active molecules containing phosphonate moieties. Case study of $BaTiO_3$." *The Journal of Physical Chemistry C*, **115**, 9850 (2011).
10. P. Kim, S. C. Jones, P. J. Hotchkiss, J. N. Haddock, B. Kippelen, S. R. Marder, and J. W. Perry, "Phosphonic acid-modified barium titanate polymer nanocomposites with high permittivity and dielectric strength." *Adv. Mater.*, **19**, 1001 (2007).
11. P. J. Hotchkiss, *The Design, Synthesis, and Use of Phosphonic Acids for the Surface Modification of Metal Oxides.* (Georgia Institute of Technology, Atlanta, GA) (2008).
12. C. W. Beier, M. A. Cuevas, and R. L. Brutchey, "Effect of surface modification on the dielectric properties of $BaTiO_3$ nanocrystals." *Langmuir*, **26**, 5067 (2010).
13. B. I. Dach, H. R. Rengifo, N. J. Turro, and J. T. Koberstein, "Cross-linked 'matrix-free' nanocomposites from reactive polymer−silica hybrid nanoparticles." *Macromolecules*, **43**, 6549 (2010).
14. C. Shi, S. J. L. Billinge, E. Puma, S. H. Bang, N. J. H. Bean, J.-C. de Sugny, R. G. Gambee, R. C. Haskell, A. Hightower, and T. C. Monson, "Barium titanate

nanoparticles: short-range lattice distortions with long-range cubic order." *Physical Review B*, **98**, 085421 (2018).

15. L. Benda, B. Schneider, and V. Sychrovsky, "Calculating the response of NMR shielding tensor sigma(^{31}P) and 2J(^{31}P, ^{13}C) coupling constants in nucleic acid phosphate to coordination of the Mg^{2+} cation." *J. Phys. Chem. A*, **115**, 2385 (2011).
16. L. Benda, Z. Sochorova Vokacova, M. Straka, and V. Sychrovsky, "Correlating the ^{31}P NMR chemical shielding tensor and the 2J(P,C) spin-spin coupling constants with torsion angles zeta and alpha in the backbone of nucleic acids." *J. Phys. Chem. B*, **116**, 3823 (2012).
17. C. van Wüllen, "A comparison of density functional methods for the calculation of phosphorus-31 NMR chemical shifts." *Phys. Chem. Chem. Phys.*, **2**, 2137 (2000).
18. P. A. Schultz, (2018), (http:/dft.sandia.gov/Quest)SeqQuest code.
19. J. P. Perdew, K. Burke, and M. Ernzerhof, "Generalized gradient approximation made simple." *Phys. Rev. Lett.*, **77**, 3865 (1996).
20. D. R. Hamann, "Generalized norm-conserving pseudopotentials." *Phys. Rev. B: Condens. Matter*, **40**, 2980 (1989).
21. S. Yoon, S. Baik, M. G. Kim, N. Shin, and I. Kim, "Synthesis of tetragonal barium titanate nanoparticles via alkoxide-hydroxide sol-precipitation: effect of water addition." *J. Am. Ceram. Soc.*, **90**, 311 (2007).
22. C. Pithan, D. Hennings, and R. Waser, "Progress in the synthesis of nanocrystalline $BaTiO_3$ powders for MLCC." *Int. J. Appl. Ceram. Technol.*, **2**, 1 (2005).
23. D. Geldof, M. Tassi, R. Carleer, P. Adriaensens, A. Roevens, V. Meynen, and F. Blockhuys, "Binding modes of phosphonic acid derivatives adsorbed on TiO_2 surfaces: assignments of experimental IR and NMR spectra based on DFT/PBC calculations." *Surf. Sci.*, **655**, 31 (2017).
24. P. H. Mutin, G. Guerrero, and A. Vioux, "Hybrid materials from organophosphorus coupling molecules." *J. Mater. Chem.*, **15**, 3761 (2005).
25. M. Mehring, M. Schurmann, and R. Ludwig, "Tert-Butylphosphonic acid: from the bulk to the gas phase." *Chemistry*, **9**, 837 (2003).
26. J. D. Baniecki, M. Ishii, K. Kurihara, K. Yamanaka, T. Yano, K. Shinozaki, T. Imada, and Y. Kobayashi, "Chemisorption of water and carbon dioxide on nanostructured $BaTiO_3$–$SrTiO_3$(001) surfaces." *J. Appl. Phys.*, **106**, 054109 (2009).
27. J. L. Kaufman et al., "Permittivity effects of particle agglomeration in ferroelectric ceramic-epoxy composites using finite element modeling." *AIP Adv.*, **8**, 125020 (2018).
28. B. Meyer and D. Vanderbilt, "Ab initiostudy of $BaTiO_3$ and $PbTiO_3$ surfaces in external electric fields." *Physical Review B*, **63**, 205426 (2001).
29. Y. Umeno, J. M. Albina, B. Meyer, and C. Elsässer, "Ab initiocalculations of ferroelectric instability in $PbTiO_3$ capacitors with symmetric and asymmetric electrode layers." *Physical Review B*, **80**, 205122 (2009).
30. D. Akbarian, D. E. Yilmaz, Y. Cao, P. Ganesh, I. Dabo, J. Munro, R. Van Ginhoven, and A. C. T. van Duin, "Understanding the influence of defects and surface chemistry on ferroelectric switching: a ReaxFF investigation of $BaTiO_3$." *Phys. Chem. Chem. Phys.*, **21**, 18240 (2019).
31. A. M. Kolpak, N. Sai, and A. M. Rappe, "Short-circuit boundary conditions in ferroelectric $PbTiO_3$ thin films." *Physical Review B*, **74**, 054112 (2006).